ADDITIVE MANUFACTURING OF BIOINSPIRED BULK GRADIENT STRUCTURES TO ENHANCE MECHANICAL PERFORMANCE

An Undergraduate Research Scholars Thesis

by

JULIA K. CARTER

Submitted to the Undergraduate Research Scholars program at
Texas A&M University
in partial fulfillment of the requirements for the designation as an

UNDERGRADUATE RESEARCH SCHOLAR

Approved by Research Advisor: Dr. Mathew Kuttolamadom

May 2018

Major: Manufacturing & Mechanical Engineering Technology

TABLE OF CONTENTS

ABSTRACT

Additive Manufacturing of Bioinspired Bulk Gradient Structures to Enhance Mechanical Performance

Julia K. Carter
Department of Engineering Technology & Industrial Distribution
Texas A&M University

Research Advisor: Dr. Mathew Kuttolamadom
Department of Engineering Technology & Industrial Distribution
Department of Materials Science & Engineering
Texas A&M University

The research objective of this project is to investigate the effects of energy density-based process parameters on the resulting mechanical properties of stainless steel 316L built by a powder-bed additive manufacturing process. More specifically, we will to elucidate how the volumetric energy density imparted by the laser as well as the energy deposition rate, affects the hardness, porosity and density of the bulk material. For this, process parameters such as laser power, and the variables constituting the effective scanning speed were changed, which effectively alters the energy density imparted onto the material. By conducting a systematic design of experiments, an understanding of the resolutions of properties achievable is obtained. The resulting structures were tested for hardness, density measurements, and underwent elemental analysis. By understanding the relationships of these mechanical properties as a function of process energy density, it will be possible to create tailored spatial mechanical property gradients. Bioinspired gradient structures can then be created and their mechanical performance evaluated.

ACKNOWLEDGEMENTS

I would like to thank my advisor, Dr. Kuttolamadom, and my research partner Yash Parikh for their guidance, support, and motivation throughout the course of this research.

Thanks also go to my friends and colleagues for making my time at Texas A&M University a rewarding experience.

NOMENCLATURE

AM	Additive Manufacturing
CAD	Computer-Aided-Design
CAM	Computer-Aided-Manufacturing
DIC	Digital Imaging Cameras
EBM	Electron Beam Melting
FGM	Functionally Graded Material
HV	Vickers Hardness Number
SEM	Scanning Electron Microscope
SLM	Selective Laser Melting
SLS	Selective Laser Sintering
SS316L	AISI 316L Stainless Steel

CHAPTER I

INTRODUCTION

Objectives

The eventual goal of this project is to be able to gain control over the high-resolution (micron-scale) spatial distribution of mechanical properties (hardness, porosity and density) within a single alloy system, and hence be able to tune their mechanical responses to external stimuli. In light of this goal, the specific objectives of the project are:

1. To investigate the effects of volumetric energy density-based process parameters and the rate of energy deposition on the resulting mechanical properties of Stainless Steel 316L structures fabricated by a selective laser melting (SLM) additive manufacturing process,
2. To establish the resolutions in mechanical property gradients achievable, and
3. To fabricate bioinspired bulk structures having spatial mechanical property gradients, and to evaluate their mechanical performance.

Thus, this project will help map energy density-based process parameters of SLM processes to the resulting mechanical properties of additive manufactured bulk structures.

Background

Combining the capability of additive manufacturing with the ingenuity of nature's tailored designs in order to create bioinspired synthetic materials is the long-term goal of this project. For this, we need to gain an understanding of how to create a functionally-gradient material by varying the energy density and manner of laser energy input into the material, leading to variations in mechanical properties. Bioinspired derivatives that will be subsequently created are expected to perform mechanically better. The ability to design and create specific

parts layer-by-layer makes it possible to change and control the material as it is built. Understanding how to tailor the process parameters to produce specific mechanical properties can greatly advance the capabilities of structural parts.

Selective laser melting (SLM) additive manufacturing

Additive manufacturing is a type of rapid prototyping process that allows for design freedoms beyond those typically achievable with traditional manufacturing processes. With the rise of metal additive manufacturing processes, there are now more options than ever to build parts. One specific type of additive manufacturing, called Selective Laser Melting (SLM), is especially popular because of the wide range of materials that can be used from polymers, to ceramics, to metals[1]. The process relies on a laser that scans a pattern through a powder bed, melting and fusing the powder together, creating a solid 3-dimensional part layer by layer. The integrity and density of the resulting parts depend greatly on the laser power, scanning speed of the laser, and many other parameters. Numerous metallic alloys have been used successfully, such as cobalt and nickel based super-alloys, titanium alloys, stainless steels, etc[2].

Stainless Steel 316L is a popular material to use with powder bed fusion processes. It has been well-researched and can be printed at near full density[3]. However, the powder bed fusion process uses a single material, with typically homogeneous properties throughout a single part. The goal of this project is to vary the density and other mechanical properties throughout a part by altering the process parameters within a single print. This project will lay the ground work of establishing a relationship between the process parameters that affect energy density and the resulting mechanical properties. This ability to control the material density (and porosity) distribution permits the ability to tailor spatial mechanical property distributions (viz., hardness);

such tailorable materials will enable us to better predict and achieve desired responses to force and temperature stimuli[4].

Bioinspired functionally-graded materials

The inspiration for this project comes from materials found in nature, such as mammalian teeth. Changes in the stiffness and hardness can be seen within and across the layers of teeth. The gradient in mechanical properties is tailored to specific functions, and without such gradients, teeth and bones would not be effective. Typically, there is a hard, outer layer that serves to withstand compression and impact. The inner layers of the teeth have decreased stiffness to avoid the overall structure being overly brittle[5]. Because of such gradients, the structure can remain flexible while still being extremely wear resistant.

Methodology

In order to change the density of the material, the energy density of the laser needs to be varied. The foremost process parameters that affect this energy density are the laser power and the effective scan speed of the laser. First, a range of values will be selected for the laser power and scan speed, based on literature. Specimen will be printed using these parameters on the Renishaw AM400 Additive Manufacturing machine. For the first print, the parameters will be changed every discretely as the part is built, so that each zone could be tested separately to quantify its resulting mechanical properties. Properties of interest include measuring hardness (using a Vickers Hardness Tester), density (using the Archimedes principle). Surface texture and elemental analysis will be respectively conducted using a surface profiler and scanning electron microscope, as well as testing and comparing porosity. Then, all the data will be consolidated and examined to find a possible combination of process parameters that result in a monotonic

gradient in mechanical properties. Finally, a true gradient material will be printed at different resolutions and tested for mechanical performance.

CHAPTER II

BACKGROUND & LITERATURE REVIEW

Additive Manufacturing

Additive Manufacturing (AM) is the process of creating three-dimensional parts in a layer-by-layer fashion, adding material rather than removing it as in traditional machining. AM is not only used for rapid prototyping, it is also being used to manufacture actual components because of its ability to reduce time and cost[1]. Specific AM processes that can produce metal parts are increasingly being used for manufacturing components in the aerospace industry. AM processes are able to create much more complex parts and profiles that are not possible with traditional machining; this flexibility in design and manufacturing options allows for creating complex shapes that can facilitate better strength-to-weight ratios[1]. It can also be utilized to manufacture near-net-shape and customizable medical apparatuses for orthopedics and dentistry[6]. AM and 3D printing are broad terms that can refer to many different processes, and which can be classified into three general categories, as show in Figure 1.

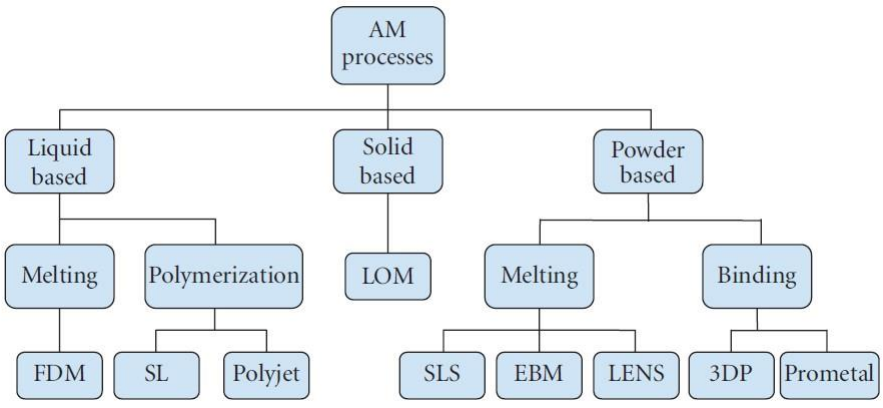

Figure 1. A breakdown of the most common AM Processes[1].

Selective Laser Melting and Process Parameters

Powder based AM processes consist of fusing pre-alloyed atomized powders using the energy of a laser; the powder particles are spherical, or near-spherical to ensure efficient flow and uniform melting[7]. In the Selective Laser Sintering (SLS) and Electron Beam Melting (EBM) processes, the powder can be compacted in a single layer on a bed, or the powder can be directly injected to a specific area, as is done in the LENS process. This study will be focusing on a powder bed, laser-based process called Selective Laser Melting (SLM).

In the SLM Process, layers of metallic powder are successively melted by the energy from a focused laser beam[6].

Figure 2 shows the schematic of the SLM Process as well as some of the relevant process parameters: laser power (P_L), the scanning speed (v_s), the layer thickness (d), and the hatch spacing (h). Lasers used for SLM can be continuous or pulsed; if a pulsed laser is used, the laser moves discretely from point to point and is turned on and off rather than scanning continuously. At each point the laser pauses and is turned on for a specified amount of time, it then moves a specified distance and pulses again. Figure 3 shows the scanning pattern of a pulsed laser, when compared to

Figure 2 the schematics show that the scanning pattern and hatch distance are not affected by the pulsed laser because the melt pool extends passed the area of the laser and overlaps to create a continuous melt pattern as shown in Figure 4.

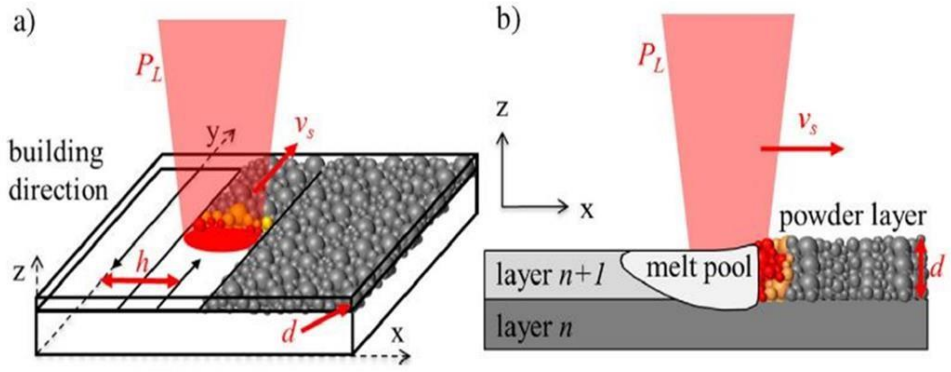

Figure 2. Schematic of the SLM process a) relevant process parameters b) melt pool[8].

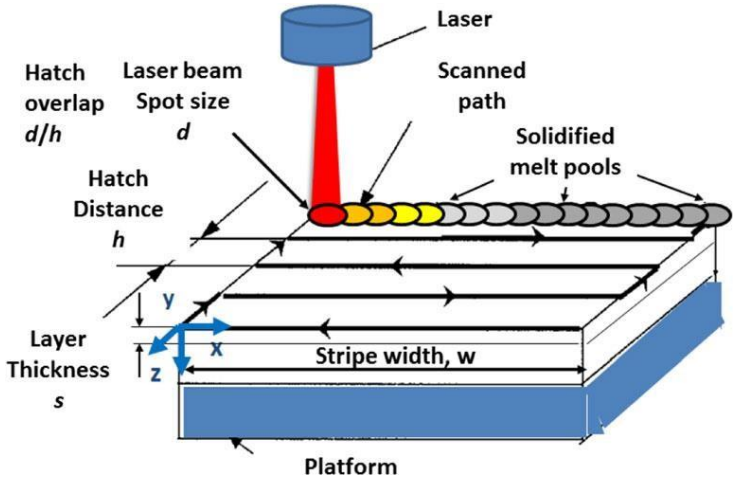

Figure 3. SLM scanning patter, showing the hatch spacing and pulsed laser melt pools[9].

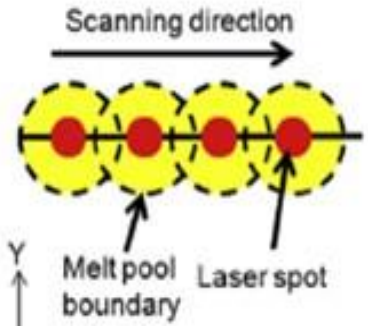

Figure 4. Pulsed laser scanning pattern: the center circle shows the area of the laser pulse, the outer and overlapping circles are the resulting melt pools[10].

The SLM process is very similar to SLS, however the temperature of the SLS process stays just above the melting point of the material, whereas the powder actually becomes molten during SLM[1]. The powder is compacted into a layer on a metal bed, after one complete pass of the laser, the bed moves down by the distance of the layer thickness. After the bed moves, a new layer of powder is deposited and the laser scans again. The entire process takes place in a chamber filled with an inert gas, such as argon, which prevents oxidation and provides efficient heat conduction and cooling[7]. Because the powder is fully melted, SLM is able to produce higher density parts with mechanical properties that are comparable to that of bulk materials; however, there is residual stress and deformation in the parts because of the continuous cycle of melting and cooling within the material[11]. The deformation and stresses within the material can be mitigated by selecting the correct process parameters for the build. More than 130 process parameters affect the final quality of the material, but the most influential are laser power, scan speed, scan strategy, and powder thickness[3]. The dimensional accuracy of the process is limited by the size and shape of the powder particles[1]. Stainless steel parts have been created with >99% density through the SLM process. High density parts have been successfully created at a laser power of 100W, but they are also possible at laser powers up to 400W. The challenge of producing high density parts at a high laser power is the selection of the proper scanning speed. Density reduces at high scanning speeds due to insufficient melting, but can also reduce at slower scanning speeds because of voids in the melt pools and gas inclusions due to localized energy deposition[3]. Studies have also been completed to relate the density to the layer thickness of the powder while power and scan speed are fixed, a layer thickness of 30μm was found to produce the highest density material[3]. The scanning strategy also heavily influences the quality and density of the material. If the laser were to scan large areas at a time, the laser beam travel

distance would be longer and the scanned tracks would have more time to cool between laser passes; consequently, the entire area would cool to lower temperatures, which affects the melting of the next layer[11]. Figure 5 shows the ideal scanning strategy for SLM, which includes scanning small areas at a time and changing the direction of scanning path at each layer to allow for uniform cooling. Each layer is only a few microns thick, this offers freedom of design at a very precise level, allowing the designer to change the outcome of the final component by finding the ideal parameter combination.

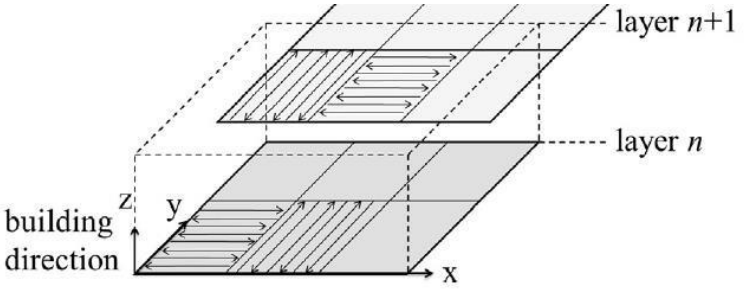

Figure 5. The ideal scanning strategy for SLM, small areas are scanned at a time and the direction of the scan pattern changes in each area[8].

Bioinspired Functionally Graded Materials

Another benefit of Additive Manufacturing is the ability to produce Functionally Graded Materials (FGMs). FGMs contain spatial gradients, with tailored mechanical properties for a specific performance or function. These spatial gradations can be created by the structure and/or the composition of the material[12]. Using AM to create FGMs allows freedoms in both design and material selection, making it possible to design internal structures that change the mechanical properties of the final component[13]. Creating compositionally graded materials by powder metallurgy involves creating a layered geometry by stacking powders of varying compositions, or using a single powder with varied control parameters[12]. FGMs are very useful

for components with specific property requirements that are not found in typical materials such as the combination of high hardness and high toughness. They are especially beneficial in applications that develop thermal stress concentrations from varying thermal expansion coefficients[12]. Figure 6 shows an example of a compositional FGM in the form of joining two materials with different thermal expansion coefficients, creating a gradient between the two materials helps relieve the stress that is created by the discrete material change[12].

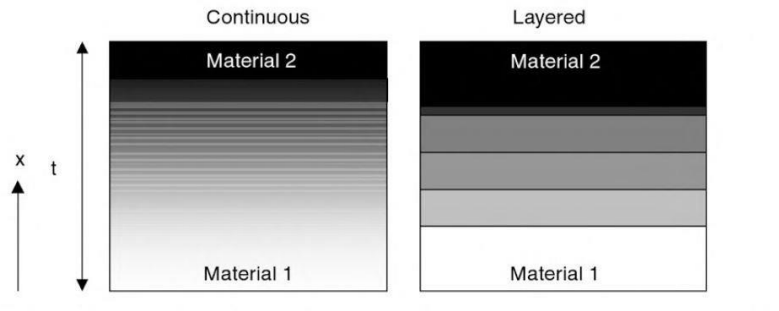

Figure 6. Comparison of joint between two materials. Architecture on the left shows a continuous gradation while the one of the rights in layered or discrete[12].

Some of the best examples of FGMs can be found in nature. For example, the human tooth, ligament and bone interfaces in the body, and the beak of a Humboldt squid are all different types of graded materials[5]. In the example of the human tooth, the outer enamel provides a hard and wear resistant coating, but the next layer of dentin and the underlying bone have lower stiffness to avoid breaking under the loads of chewing. This change in stiffness is achieved by the varying levels of minerals incorporated into the material, making the tooth a compositional FGM. Figure 7 shows the range of stiffness values observed in the different layers of a typical tooth.

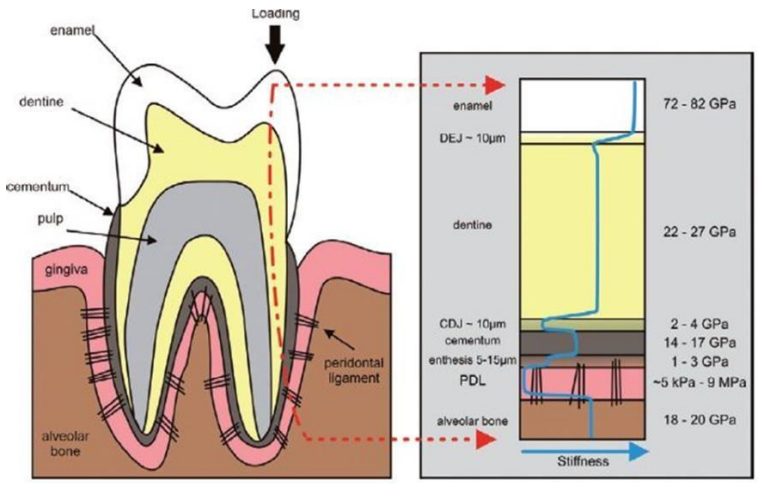

Figure 7. Cross Section of Human Tooth, Indicating the Major Layers. The Diagram on the Right Shows the Stiffness Variation Passing Through the Different Layers[5].

The biomedical industry is constantly looking for newer and better materials for things like bone replacement. The human bone is complex structure with a dense outer layer and an inner spongy region, making it a perfect candidate for a FGM[13]. Titanium is typically used because it is biocompatible and has high strength, but that means it is also much heavier than a typical human bone. One way to reduce this weight is to create cellular structures rather than using a solid material, these manufactured pores reduce the weight while maintaining strength, making it a structural FGM[13]. There are countless examples of gradient properties in nature, both structurally and compositionally, and one of the best ways to mimic these structures is to create FGMs through additive manufacturing. Adding complexity to the geometry of a structure allows for the varying of mechanical properties in different regions of a single component, which is the main inspiration for this study of enhancing mechanical properties.

CHAPTER III

MATERIALS & METHODS

Stainless Steel 316L

In this study, stainless steel parts are fabricated by the SLM process. AISI 316L (SS316L) is an austenitic stainless steel with a very low carbon content and great corrosion resistance[14]. SS316L is also known for its weldability and machineability. SS316L, by definition, contains a maximum of 0.03% Carbon by mass, which is a much lower that the carbon levels found in SS316. The typical tensile strength and yield strength of SS316L are 485MPa and 170MPa respectively and the hardness is 95 on the Rockwell B scale, which translates to 218 on the Vickers Hardness scale[15]. These properties are typical of bulk SS316L, which has a density of 8g/cm^3. SS316L is an ideal material for SLM because it creates parts with higher strength and lower ductility than casted 316L. SLM has a high cooling rate which lends to the creation of a typical microstructure for stainless steel[16]. The metallic powder of AISI 316L stainless steel has a particle size below 50 µm and a mean particle size between 10 µm to 45 µm. The powder composition is listed in Table 1. Figure 8 shows an SEM image of the SS316L powder that was used in this study powder particles are typically spherical or near-spherical in shape.

Table 1. Chemical composition of 316L stainless steel powder (wt. %)

Cr	Ni	Mo	Mn	Si	N	P	C	S	Fe
16-18	10-14	2-3	2 max	1 max	0.1 max	0.045 max	0.03 max	0.03 max	Bal.

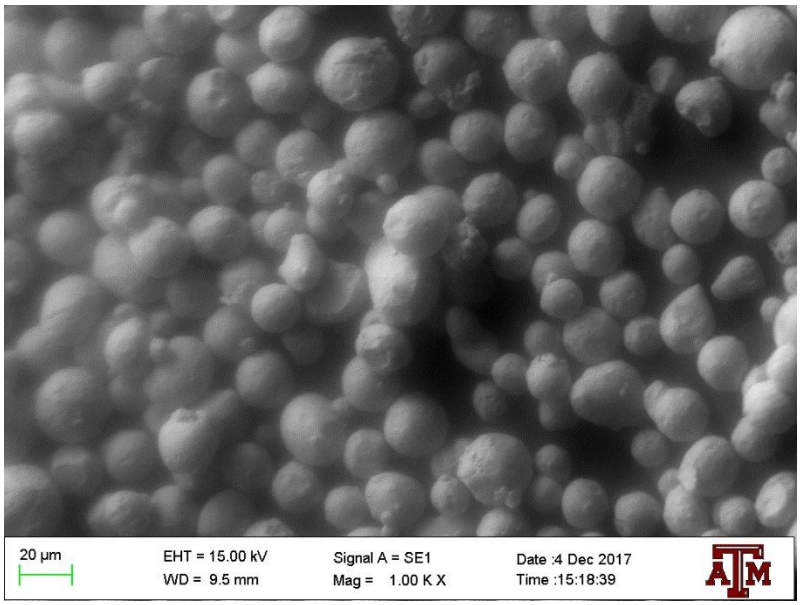

Figure 8. SEM Image of SS316L atomized powder.

Machine Specifications

The machine shown in Figure 9 is the Renishaw AM400 SLM System. This system is equipped with a maximum laser power of 400 W and employs an ytterbium fiber laser with a wavelength of 1070 nm. The laser beam (spot) diameter is approximately 70 µm and its profile is Gaussian (TEM00). The system uses argon as an inert gas to keep the oxygen level of below 500 ppm, which prevents oxidation effects on the parts. The system specifications are summarized in Table 2.

Figure 9. Renishaw AM400.

Table 2. A summary of the relevant process parameters on the Renishaw AM400.

Parameter	Description
Additive manufacturing system	RENISHAW AM400
Software package(s)	SOLIDWORKS 2016 / QuantAM
Powder description	Gas atomized 800 mesh 316L stainless steel powder (99% purity)
Powder grain size	~50 µm (spherical morphology)
Powder apparent density	7.99 g/cm^3
Layer thickness	50 µm
Inert Gas	Argon (zero grade)
Laser	Pulse type

The Renishaw AM400 is programmed using the software QuantAM, which is provided by Renishaw. QuantAM is a type of CAM software that allows the user to import a CAD model and select the relevant process parameters. The software outputs a computer code that specifies

the scanning path for the laser and other machine controls. As shown in Figure 10, QuantAM shows a preview of the build layers and scan patterns. The user also defines support structures in the QuantAM software, the structures are built underneath the intended parts at a specified height. Support structures are typically used with all parts to ease the process of removing the parts from the steel print bed, they are also placed under detailed parts to support overhangs or abnormal features, [17].

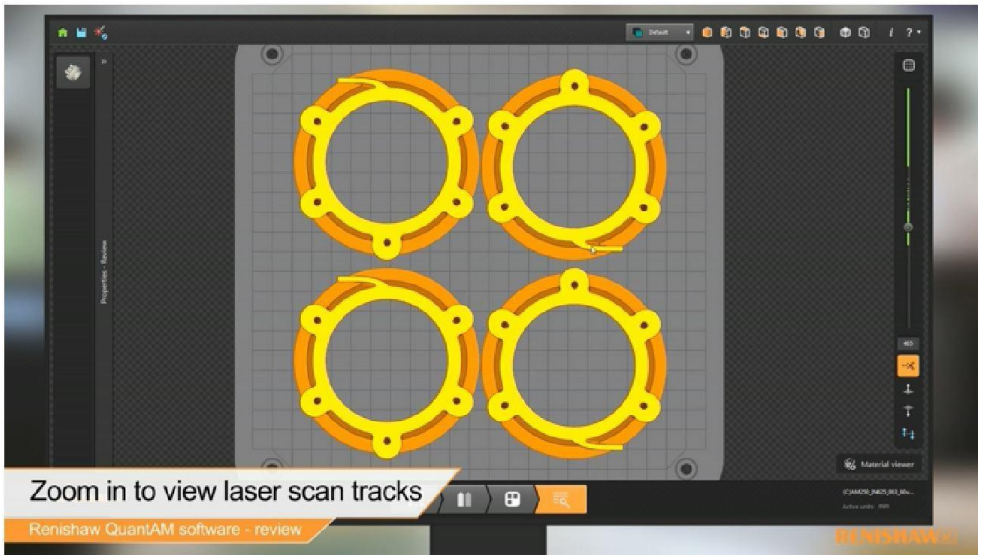

Figure 10. Renishaw QuantAM Graphical User Interface.

Preliminary Work

For the first round of tests, cylindrical bars, oriented horizontally on the print bed, are created using a range of process parameters. Figure 11 shows a layout of the print, as rendered in QuantAM. Cylindrical tensile bars were needed for other testing and were printed using the standard process parameters, and then new sections were added to the ends with varied process parameters. The numbers on the parts represent each section where the process parameters were varied, and the pattern on the inside of each part represents the support material that is built under the parts. Part numbers 1-7, 10-16, 18-24, and 26-32 are relevant to this study. Figure 12

shows a photograph of the SLM Process mid print. The powder is shown over the entire print bed and the laser has partially scanned the pattern. This is roughly midway through the printing process, so there are solid parts already formed underneath the top layer of powder that is being scanned. In this experiment, 2 mm support structures are built underneath each bar, to allow for easier removal from the print bed without damaging the parts. Figure 13 shows the cylindrical bars and the support structures on the print bed after printing has been completed.

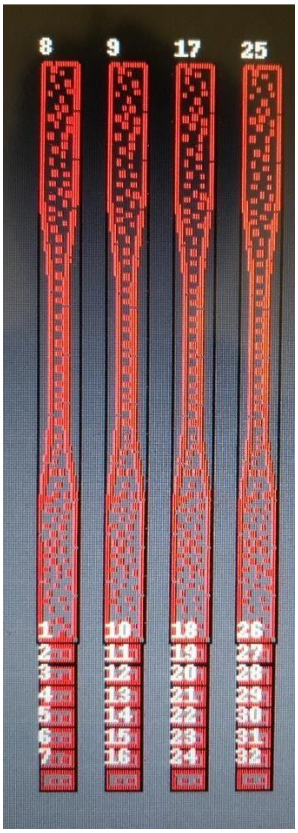

Figure 11. Print Layout as rendered in QuantAM.

Figure 12. Photo of SLM System mid-print.

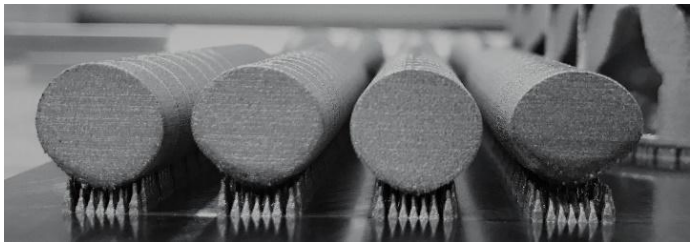

Figure 13. The cylindrical bars created by SLM and the 2mm support structures.

After the bars are printed on the Renishaw AM400 system, they are removed from the print bed and cut into sections using a Wire EDM. Each section had a length of 7 mm, a thickness of 5 mm, and width of 5 mm, as shown in Figure 14. Each specimen was then polished to be used for density and hardness testing. The testing procedures are discussed in greater detail in a later section.

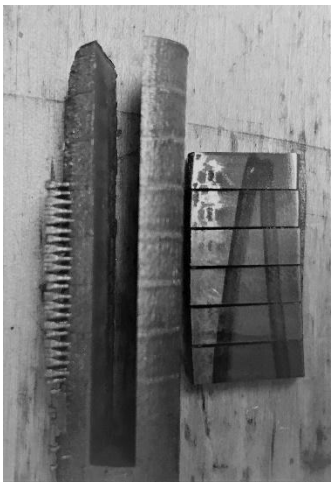

Figure 14. The sections that were cut from each specimen.

Process parameter selection

To study the effect of energy density parameters on the mechanical properties of the SS316L parts, laser power and scanning velocity are varied. Twenty-eight different combinations of the two parameters are used while printing the specimen. The selected parameters for the laser power and scanning velocities are calculated based on the energy density that is applied to the material during the melting process. Energy density (J/mm^2) is calculated based on laser power, scanning velocity, and hatch distance as shown in Equation 1. Where P (W) is the laser power, v (mm/s) is the laser scanning velocity, and r is the laser spot diameter (mm).

$$E = \left[\frac{P}{\pi r^2}\right]\left[\frac{2r}{v}\right] \quad (1)$$

For this study, power and scanning velocity are varied, while spot diameter, layer thickness and hatch spacing remain constant at 70 µm 50 µm, and 110 µm respectively. Since the area was held constant, the energy density that is transferred to the material depends on the material interaction time (affected by power and scanning velocity), so P/v is also a relevant

parameter. Since the AM400 uses a pulsed laser, we used the exposure time to calculate the effective scanning speed using Equation 2.

$$Speed = \frac{60}{exposure\ time + 12} \times 10^3 \quad (2)$$

Increasing laser power or decreasing scanning velocity leads to a higher energy density and complete melting because of superior particle fusion[18]. Increasing energy density leads to larger melt pools and reduced porosities, both of which ultimately improve the density of the manufactured parts. There is a specific range of energy density that produces adequate melting, if the density is too high it may lead to evaporation of metal powder and the formation of plasma, this can create voids that increase porosity to unacceptable rates[3]. Also, if the energy density is too low, it will result in inefficient melting and bonding of the powders and will not produce complete parts. The process parameters were varied as much as possible while keeping the energy density within the acceptable range.

Table 3 shows the process parameters that were chosen, the laser power was increased from 150W-250W and the exposure time was varied from 60µs-110µs, which changed the effective scanning speed from 500mm/s-800mm/s. According to Renishaw, the ideal parameter combination is 200W and 80µs, therefore the parameters are chosen around these nominal values. The sample numbers follow the numbering system from Figure 11.

Table 3. Process Parameter Combinations.

Sample Number	Power (W)	Exposure Time (s)	Speed (mm/s)	P/v (J/mm)	E(J/mm^2)
1	175	92	577	0.30	1592
2	175	108	500	0.35	1592
3	150	63	800	0.19	1364
4	150	71	723	0.21	1364
5	150	80	652	0.23	1364
6	150	92	577	0.26	1364
7	150	108	500	0.30	1364
10	200	88	600	0.33	1819
11	200	92	577	0.35	1819
12	200	97	550	0.36	1819
13	200	108	500	0.40	1819
14	175	63	800	0.22	1592
15	175	71	723	0.24	1592
16	175	80	652	0.27	1592
18	200	65	779	0.26	1819
19	200	68	750	0.27	1819
20	200	71	723	0.28	1819
21	200	74	698	0.29	1819
22	200	77	674	0.30	1819
23	200	80	652	0.31	1819
24	200	84	625	0.32	1819
26	250	80	652	0.38	2274
27	250	92	577	0.43	2274
28	250	108	500	0.50	2274
29	225	71	723	0.31	2046
30	225	80	652	0.35	2046
31	225	92	577	0.39	2046
32	225	108	500	0.45	2046

Testing procedures

After separating the printed specimen by wire EDM, each individual piece characterizes a different set of process parameters and can be tested to find the properties created by those process parameters. First, each piece is polished to an acceptable surface finish for Vickers hardness testing and SEM imaging (3-4 µm). Then, a randomly chosen specimen was analyzed under the SEM to view the structure. The goal of SEM was to determine if the change in density of the parts was due to incomplete melting of the SS316L powder, which would cause poor structural integrity. As shown in Figure 15, there are a few pores, but the majority of the microstructure is solid. The mark shown on the right side of the frame is a surface defect, which can also be seen by the naked eye in Figure 16. If more than 50% of the microstructure was pores, it would be clear that the change in part density had affected the structural integrity of the stainless steel. Figure 16 shows the polished specimen and the surface defect on the sample, which was caused by the cutting operation.

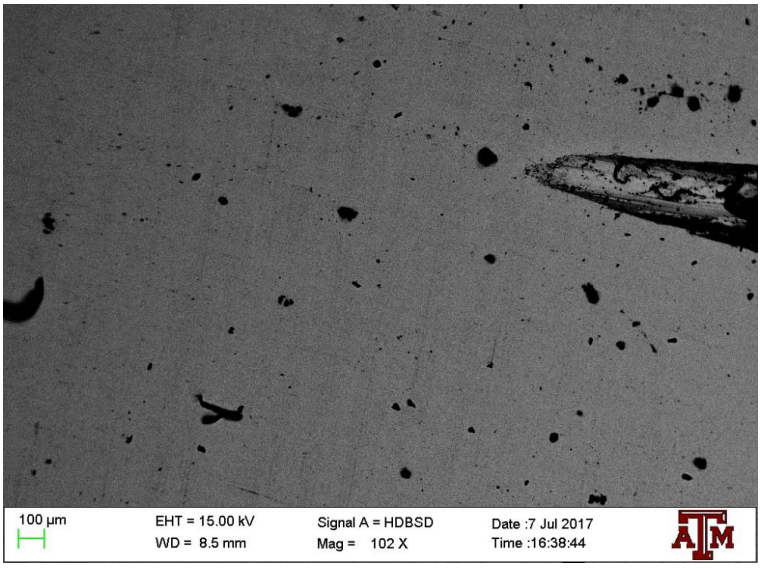

Figure 15. SEM image of specimen, the black spots show minimal porosity. The defect on the right side of the frame is a surface defect.

Figure 16. Cross section of three specimen before being separated, surface is polished and used for SEM Imaging.

The density of each piece is tested using the Archimedes principle. Each specimen is weighed dry, and then placed in a beaker of water and weighed. The water is held at a constant temperature of 23.1ºC and the density is 0.9975 g/cm^3. The density of the stainless-steel specimen is calculated by dividing the mass of the specimen in water by the volume of water displaced. The relative density is expressed as the percentage of the nominal density of SS316L powder (7.99 g/cm^3). The set-up used to weigh the specimen is shown in Figure 17. The optimal density of additively manufactured SS316L is 7.99 g/cm^3, and the goal of this project was to vary the relative density as much as possible without creating voids in the material. The results are expressed in Table 4.

Figure 17. Density Testing Set-Up

Table 4. Density Testing Results.

Sample Number	WET Sample Mass (g)	Volume of Sample (cm^3)	Density of Sample (g/cm^3)	Relative Density
1	1.257	.18	7.845	98.19
2	1.324	.19	7.812	97.77
3	1.202	.19	7.254	90.78
4	1.263	.19	7.662	95.89
5	1.352	.20	7.831	98.01
6	1.375	.20	7.910	99.00
7	1.381	.20	7.915	99.06
10	1.328	.19	7.892	98.77
11	1.351	.20	7.768	97.23
12	1.371	.20	7.838	98.10
13	1.383	.20	7.895	98.81
14	1.359	.20	7.699	96.35
15	1.387	.20	7.827	97.96
16	1.397	.20	8.000	100.12
18	1.672	.24	7.886	98.70
19	1.649	.24	7.847	98.21
20	1.874	.28	7.811	97.76
21	1.243	.18	7.790	97.50

Table 4. cont. Density Testing Results.

Sample Number	WET Sample Mass (g)	Volume of Sample (cm^3)	Density of Sample (g/cm^3)	Relative Density
22	1.596	.23	7.858	98.35
23	1.748	.26	7.765	97.19
24	1.580	.23	7.772	97.28
26	1.215	.18	7.858	98.35
27	1.283	.18	7.985	99.93
28	1.311	.19	7.942	99.40
29	1.343	.19	7.915	99.06
30	1.363	.20	7.899	98.87
31	1.373	.20	7.878	98.59
32	1.378	.20	7.929	99.23

The hardness of the stainless steel is determined using a Vickers Hardness Tester, similar to the one shown in Figure 18. The hardness testing process followed ASTM Standard E92 and used a square-based pyramidal diamond indenter with a force of 0.5 kgf[19]. After indenting the material, the system measures diagonal distances of the indentation and outputs the Vickers Hardness values (HV). Figure 19 shows the shape of the indenter and the shape of the indentation. Each piece was indented twice and the average was calculated and recorded. The average hardness values are shown next to the relative density in Table 5.

Figure 18. Vickers Hardness Tester.

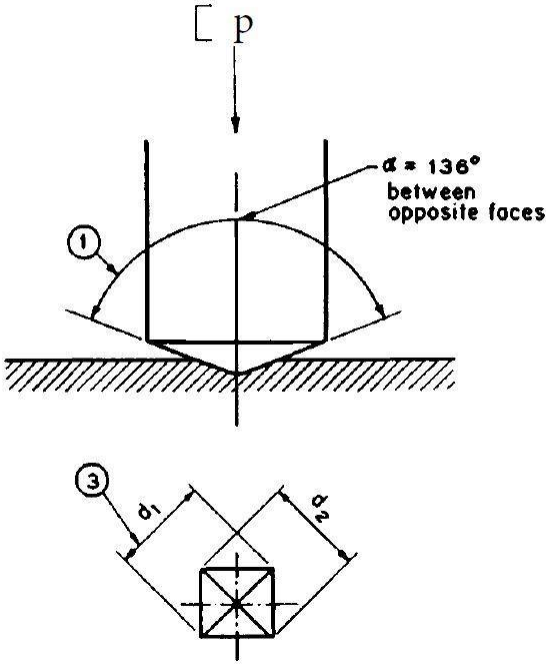

Figure 19. Hardness Indenter According to ASTM E92[19].

Table 5. Hardness Test Results.

Sample Number	Average HV	Relative Density (%)
1	266.15	98.19
2	302.05	97.77
3	294.1	90.78
4	246.95	95.89
5	262.65	98.01
6	260.75	99.00
7	284	99.06
10	277.85	98.77
11	256.4	97.23
12	282.9	98.10
13	266.4	98.81
14	209.15	96.35
15	262.05	97.96
16	262	100.12
18	259.9	98.70
19	270.75	98.21
20	272.75	97.76
21	317.9	97.50
22	269.4	98.35
23	260.85	97.19
24	257.85	97.28
26	266.8	98.35
27	269.7	99.93
28	266.45	99.40
29	275.8	99.06
30	260.5	98.87
31	267.85	98.59
32	279.2	99.23

The results from the tests showed significant variance in the hardness and the density of the different pieces. From the selected power levels and scanning speeds, the density ranged from 90.78% to 100% and the hardness levels ranged from 209.15 to 317.9 on the Vickers Hardness scale. Figure 20 shows the total range of density versus the velocity of the laser and Figure 21 shows the average hardness versus the scanning velocity, the data points are separated by the power levels.

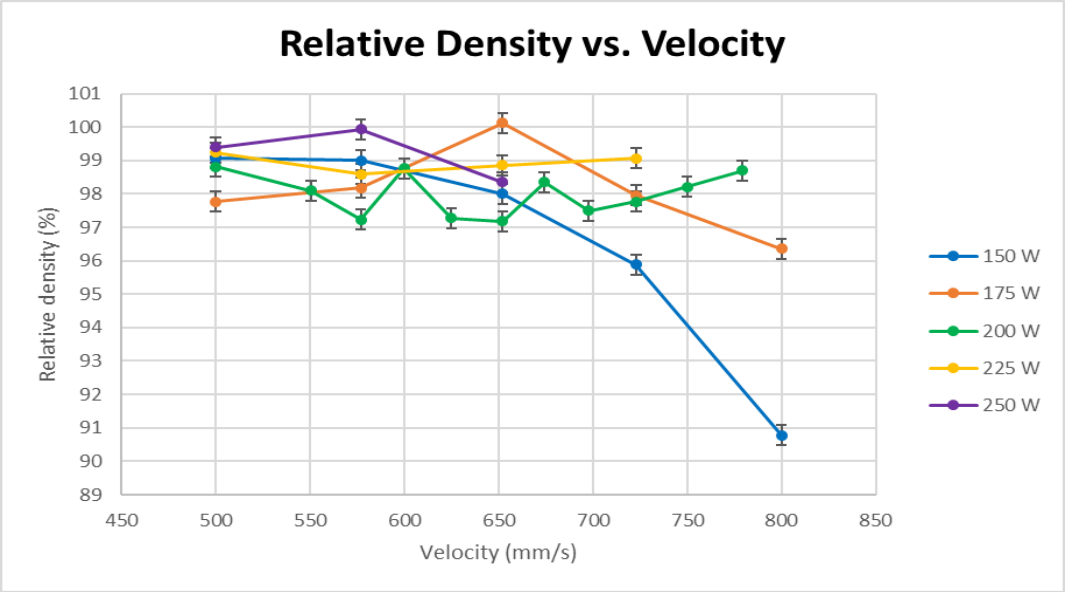

Figure 20. Relative Density vs. Velocity, separated by the different Power levels.

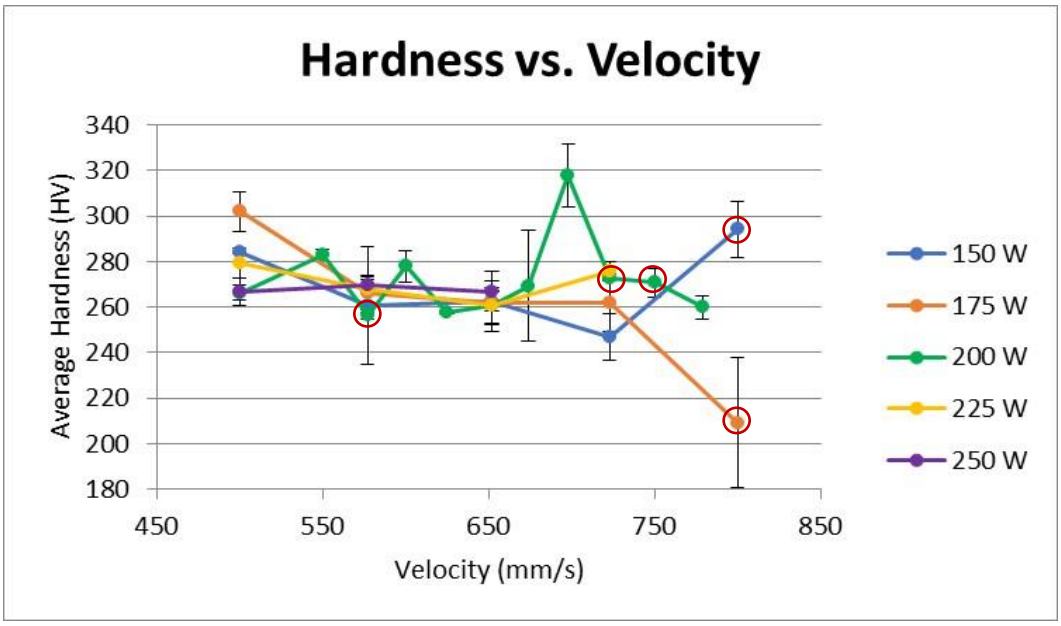

Figure 21. Average Hardness vs. Velocity, the data points circled in red are used for further testing.

Results have shown that the lower hardness values are the result of increasing the scanning velocity or reducing the laser power. It can be also noted that the energy density has a significant role to play on the mechanical properties of the final parts. This is in agreement with the experimental results. Moreover, the lower scanning velocities lead to higher density, thereby improving the macro-mechanical properties of the material.

From these results, five data points were chosen from the original data set to create a gradient. The points chosen include the samples with the highest and lowest hardness values. The hardness values and their process parameters are shown in Table 6.

Table 6. Hardness Values and Process Parameters Chosen to Create Gradient.

Sample Number	**Power (W)**	**Exposure Time (µs)**	**Speed (mm/s)**	**P/v (J/mm)**	**E(J/mm^2)**	**Hardness (HV)**
21	200	74	698	0.29	1819	317.9
3	150	63	800	0.19	1364	294.1
19	200	68	750	0.27	1819	270.75
11	200	92	577	0.35	1819	256.4
14	175	63	800	0.22	1592	209.15

CHAPTER IV

RESULTS & ANALYSES

For this round of printing, the different process parameter sections are oriented vertically and printed in the shape of a tensile test specimen. The three specimens are shown on the print bed in Figure 22. The ends of the specimens were printed with the ideal parameter combination of 200W and 80 µs, the gage length is printed with the varying process parameter detailed in Table 6. As each section is added in to the QuantAM software, the laser scan path is designed to slightly overlap with the previous section. This was done to avoid a sharp transition between process parameters because a sharp transition would likely result in a weak bond at the intersection of different process parameters.

Figure 22. Tensile Test Specimen on Print Bed.

The shape of the specimen was chosen to be suitable for micro-tensile testing and the use of Digital Imaging Correlation (DIC) software. The goal of this print was to determine if the different hardness values could be stacked on top of each other to create a gradient, while changing the process parameters at different increments. Three different sizes were printed to test the possible resolution of the gradient of the mechanical properties. The first specimen was designed according to the ASTM Standard E8 for Tensile Testing of Metallic Materials, the next two specimens were reduced to 50% and 32% of the standard specimen size[20]. The large and medium specimen were then used for testing, but the dimensions of the smallest specimen were not adequate to complete testing. The dimensions (in mm) of each specimen are shown in Figure 23, Figure 24, and Figure 25. Five different parameter combinations are used in each gage length, for example on the large specimen, the overall gage length is 25 mm, and the process parameters changed every 5 mm. The sections are labeled 1-5, left to right and the section numbering system remains consistent in all 3 specimens, the relating process parameters are detailed in Table 7. Section 6 represents the ends of the tensile test specimen which were created using the recommended settings according to Renishaw.

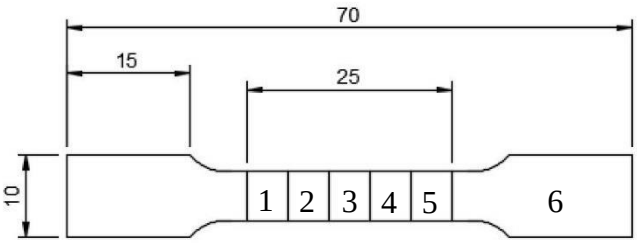

Figure 23. Large Specimen, thickness of 6 mm.

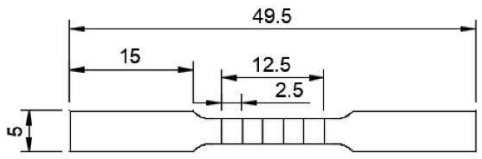

Figure 24. Medium Specimen, thickness of 3 mm.

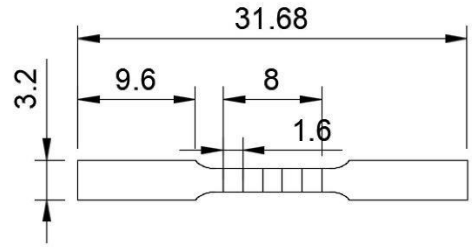

Figure 25. Small Specimen, thickness of 1.92 mm.

Table 7. Process parameters of individual sections.

Sample Number	Power (W)	Exposure Time (µs)	Speed (mm/s)	P/v (J/mm)	E(J/mm^2)	Hardness (HV)
6	200	80	652	0.31	1819	260.85
5	200	74	698	0.29	1819	317.9
4	150	63	800	0.19	1364	294.1
3	200	68	750	0.27	1819	270.75
2	200	92	577	0.35	1819	256.4
1	175	63	800	0.22	1592	209.15

Hardness Testing

Vickers hardness measurements were taken along each specimen, again using a load of 0.5 kgf. The sample is indented with the same square-based pyramidal diamond, and then the indentation is measured under the microscope. The testing system in shown in Figure 26, and the indentation is shown in Figure 27.

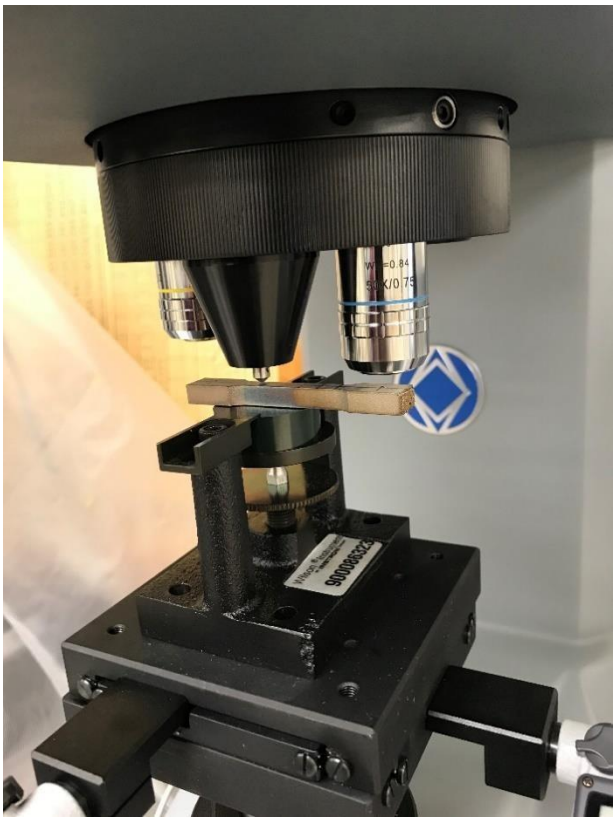

Figure 26. Vickers Hardness Testing System.

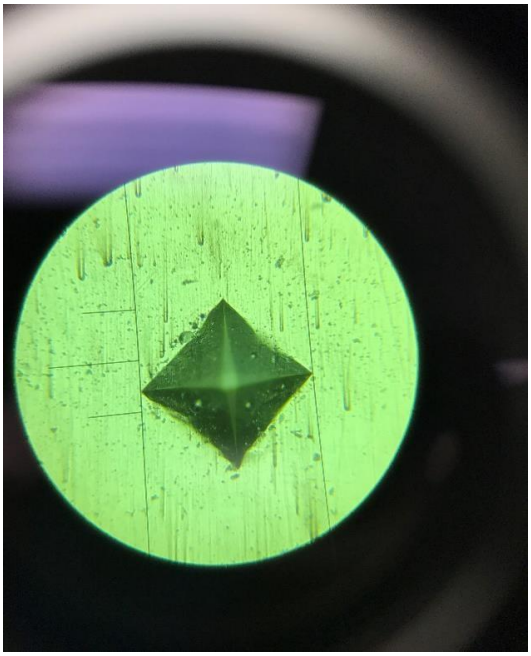

Figure 27. Hardness Indentation.

Two measurements are taken before tensile testing in each region of different process parameters, as well as at the intersections of the sections. The values are averaged and the standard deviation is documented, the results are summarized and placed next to the target hardness values from the preliminary work in Table 8. This process is repeated for each section after tensile testing and the results are shown in Table 9, the measurements are not taken at then intersections because the regions are difficult to locate after the deformation caused by tensile testing. The three hardness values from preliminary work, pre-tensile test, and post-tensile test are compared in Figure 28.

Table 8. Medium Specimen Hardness Test Results (Pre-Tensile Test)

Section	HV 1	HV 2	AVG HV	Std.	Target HV
1	244	230	237	7	209
1_2	262	236	249	13	n/a
2	258	256	257	1	256
2_3	225	232	228.5	3.5	n/a
3	260	232	246	14	271
3_4	236	244	240	4	n/a
4	255	260	257.5	2.5	294
4_5	216	213	214.5	1.5	n/a
5	245	244	244.5	0.5	318
5_6	249	233	241	8	n/a
6	257	254	255.5	1.5	261

Table 9. Medium Specimen Hardness Test Results (Post-Tensile Test).

Section	HV1	HV2	Avg HV	Std.
1	208.3	203.9	206.1	2.2
2	257.4	251.3	254.35	3.05
3	270.6	272	271.3	0.7
4	293.5	298.9	296.2	2.7
5	227.8	301.7	264.75	36.95
6	169.7	178.6	174.15	4.45

Figure 28. Hardness Results by Section for Pre-Tensile Test, Post-Tensile Test, and Preliminary Work.

As shown in Figure 28 pre-tensile and post-tensile hardness values have similar monotonic trends and are also similar in magnitude. These values were also relatively close to the target values from the preliminary work. This shows that we were able to accurately recreate the desired hardness values by manipulating the process parameters.

Tensile Testing

Tensile Testing was completed on the MTS Insight system shown in Figure 29. The test was completed using the pneumatic grips in Figure 30. Pneumatic grips are used to minimize the torsion felt by the sample when tightening the grips. The testing was recorded and analyzed using Digital Imaging Correlation (DIC) software.

Figure 29. MTS Insight Mirco-Tensile Testing System.

Figure 30. Specimen in Tensile Test Grips.

Digital Imaging Correlation (DIC)

DIC is a non-intrusive measurement system, in which the system tracks points on a plane to determine the movement and deformation of the plane. DIC is able to track individual points because it requires a non-repetitive, isotropic, high contrast pattern, as described in Figure 31. For this study, a random speckle pattern created by a white background and black speckles was used, the specimen with speckle pattern is shown in Figure 32. The camera captures a 9x9 pixel image, which is a matrix of the natural integers on the gray scale. The DIC set-up includes extra lighting and three high-resolution cameras that can be used with any tensile testing system. An example of the DIC set up is shown in Figure 33. From the data recorded by the DIC, contour plots show the stress in the specimen during tensile testing, and strain can be calculated.

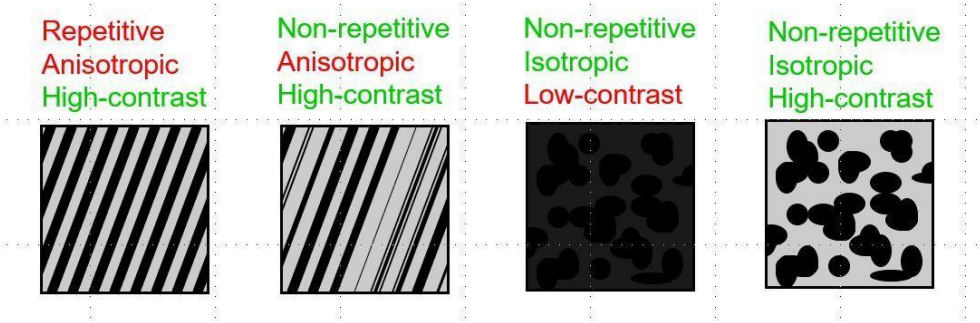

Figure 31. DIC Pattern Description.

Figure 32. Speckle Pattern Specimen.

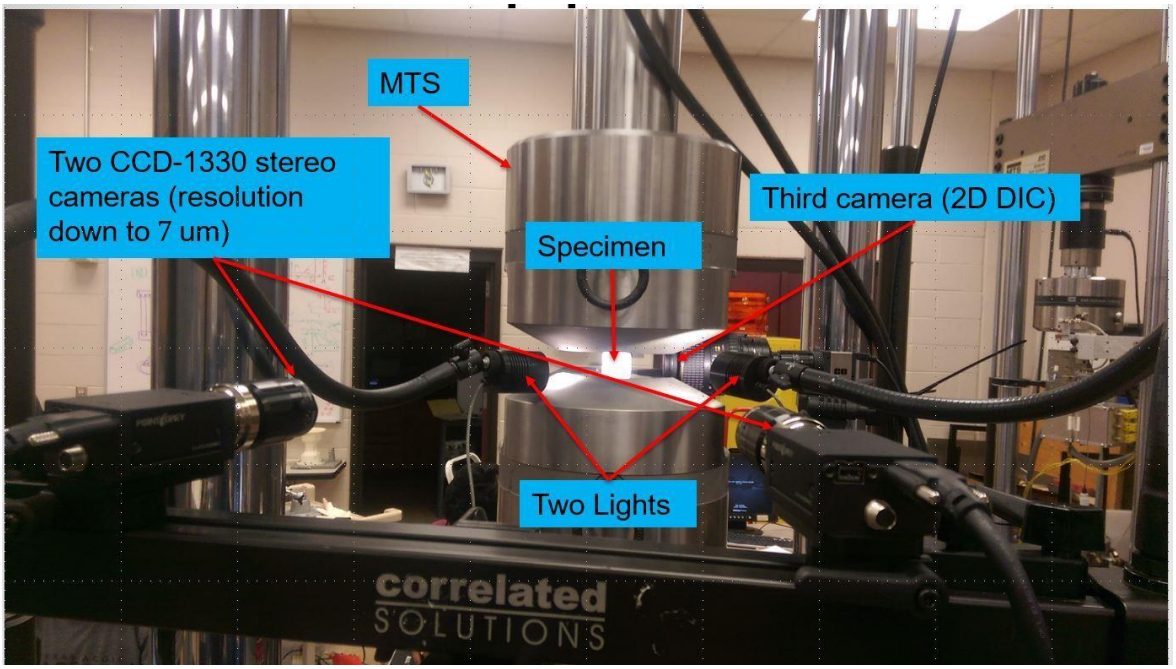

Figure 33. Digital Imaging Correlation Set-Up.

Tensile test results

The results of the tensile test showed different elongation in the regions created with different process parameters. Figure 34 shows the 3 stages of the tensile test of the large specimen. Figure 35 shows the contour plots that were captured by the DIC system, the color scale represents the relative strain values felt by the specimen at a given point in time. The first plot is before the load is applied, the entire sample is green because there is no strain, this plot shows the approximate location of the different sections. The next plots show the difference in the strain values in the different regions. Each plot is auto-scaled, so the region with the relative highest amount of deformation at that point in time is shown in red. The rate of displacement is initially highest in the bottom region, in section 1. Over time, the highest strain 'jumps' to sections 4 and 5, where the sample eventually fractures. The abrupt (and noticeable) shift in the maximum-strained regions could be due to strain hardening of the lower region. As the load is

applied, region 1 deforms more than other regions, and it accumulates plastic deformation which could possibly increase cause strain hardening and hence increase the strength in that region. As the strength increases, the deformation decreases, meaning that the highest rate of deformation is now in sections 4 and 5, where the strain continues to increase until the specimen fractures. In the stress-strain curve of the medium sample in Figure 36, we can see the linear relationship between the stress and strain which is the modulus of elasticity (Young's modulus). The modulus of elasticity of the medium sample was about 7356.6 MPa. The peak force applied to the specimen before it broke was 5775 N and the maximum stress felt by the specimen was 385.0 MPa. The maximum strain, which is the overall deformation felt by the specimen was 0.137 mm. The typical yield strength of full density SS316L is 485 MPa and the Young's modulus is 193 GPa. The values found of the medium specimen in this study are lower than that of typical SS316L because these specimens were not created at full density. The average density produced by theses process parameters is 95.8% of full density SS316L. The objective of this work was to vary the mechanical response of these specimen, which was achieved.

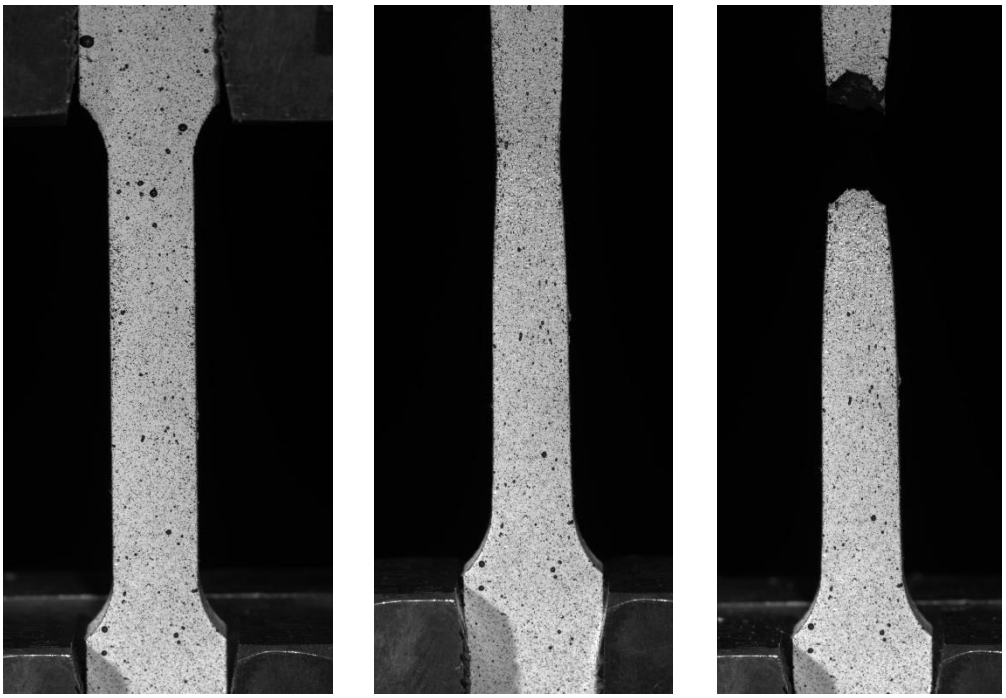

Figure 34. Tensile Test of Large Specimen.

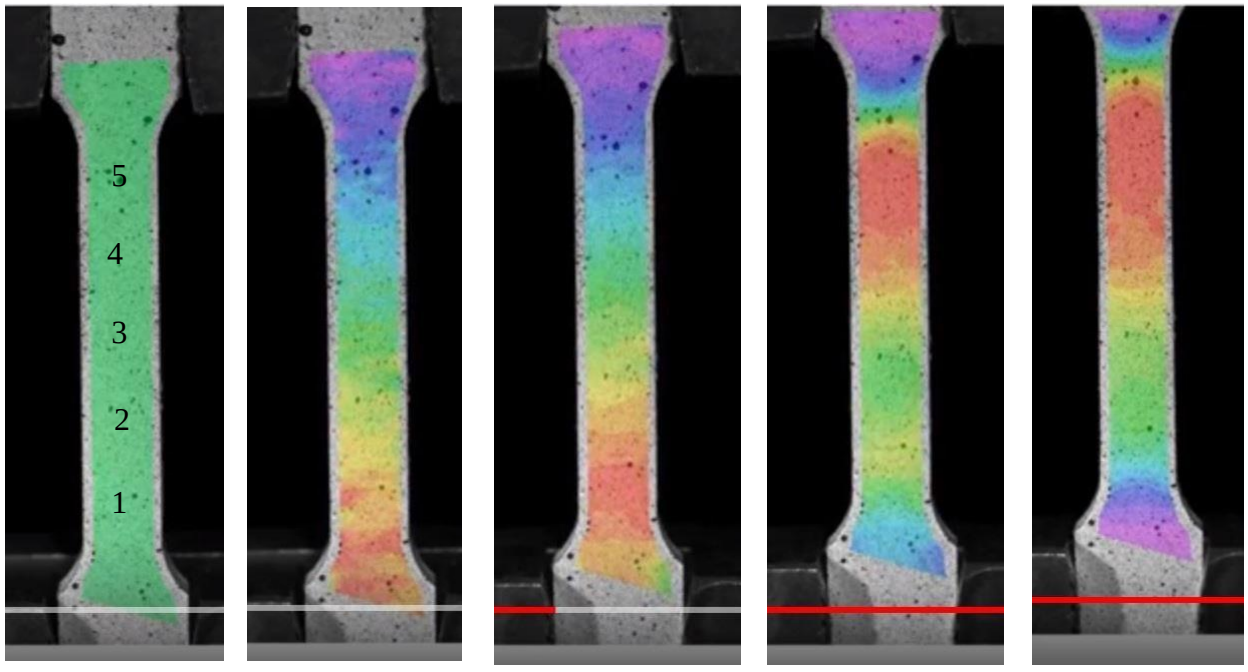

Figure 35. Contour Plots of Tensile Test of Large Specimen. The first image shows the approximate location of each section.

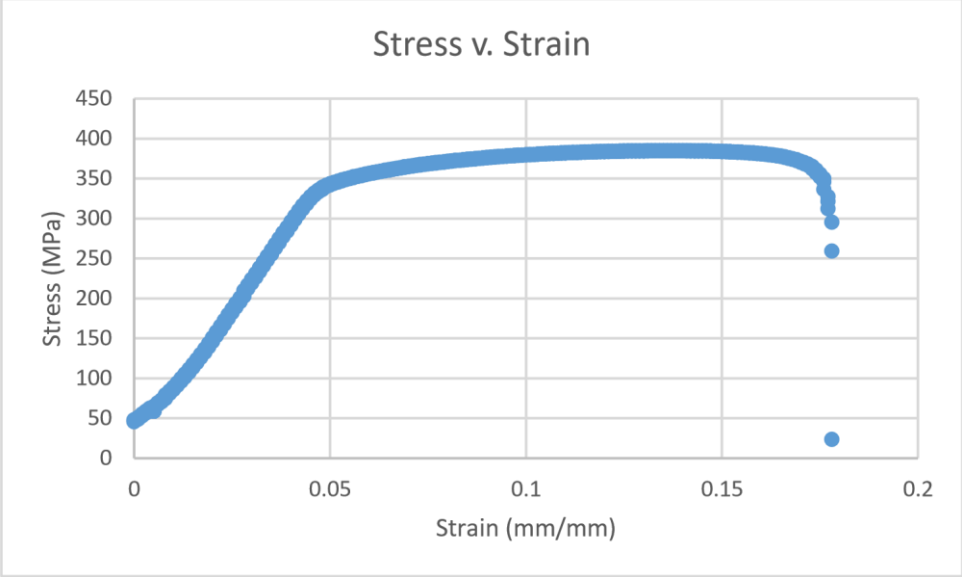

Figure 36. Stress v. Strain Plot for Medium Specimen.

From the hardness and tensile results, we were able to specify and achieve gradients in mechanical properties at different resolutions. Three resolutions were created, while the testing results of the mid-range resolution are detailed in this study, the other two resolutions showed similar results. Future work will include detailing the results of these process parameter combinations on the resulting mechanical properties at increasingly smaller resolutions. At smaller resolutions, it is possible to create a FGM with a more continuous gradient as opposed to the discrete gradients that are discussed above. The results obtained in this study are expected to help predict the various mechanical responses to thermos-mechanical input stimuli.

CHAPTER V

CONCLUSION & FUTURE WORK

The research objective of this project was to investigate the effects of energy density-based process parameters on the resulting mechanical properties of stainless steel 316L built by a powder-bed additive manufacturing process. For this, process parameters such as power and the effective scanning speed of the laser was changed, which effectively altered the volumetric energy density imparted onto the material. The resulting structures were then tested for hardness, density, and tensile strength and underwent structural analysis. Gradients at three different resolutions were created and tested to determine the resolution of gradients achievable.

The inspiration for this work came from functional gradients found in nature, such as human teeth. Changes in the stiffness and hardness can be seen throughout the layers of teeth. The gradient in mechanical properties is tailored to specific functions, and without such gradients, teeth and bones would not be effective. The next step to continue this work would be to create a stainless-steel part that mimics the structure and function of human teeth or other gradients in nature.

From the preliminary work, the range of possible hardness and density values was determined, where the process parameters were changed in 7 mm zone increments. In the next round of testing, select sets of process parameters were changed in smaller increments of 5 mm, 2.5 mm and 1.25 mm. During the tensile testing, the gage length of the tensile specimen was made of different process parameters. The results from the tensile test, was analyzed using a Digital Imaging Correlation set up, which showed that the different regions of the gage length have different properties and deformations.

By understanding the relationships of these mechanical properties as a function of process energy density, it is possible to create tailored mechanical property gradients. Thus, this project has helped to map the energy density-based process parameters of SLM processes to the resulting mechanical properties of additive manufactured structures.

REFERENCES

1. Wong, K.V. and A. Hernandez, *A Review of Additive Manufacturing.* ISRN Mechanical Engineering, 2012. **2012**: p. 1-10.

2. Murr, L.E., et al., *Fabrication of Metal and Alloy Components by Additive Manufacturing: Examples of 3D Materials Science.* Journal of Materials Research and Technology, 2012. **1**(1): p. 42-54.

3. Kamath, C., et al., *Density of additively-manufactured, 316L SS parts using laser powder-bed fusion at powers up to 400 W.* The International Journal of Advanced Manufacturing Technology, 2014. **74**(1-4): p. 65-78.

4. Pierre, M., H. Jean-Yves, and M. Pascal, *Toolpaths for additive manufacturing of functionally graded materials (FGM) parts.* Rapid Prototyping Journal, 2014. **20**(6): p. 511-522.

5. Dunlop, J.W.C., R. Weinkamer, and P. Fratzl, *Artful interfaces within biological materials.* Materials Today, 2011. **14**(3): p. 70-78.

6. Yang, Y., et al., *Accuracy and density optimization in directly fabricating customized orthodontic production by selective laser melting.* Rapid Prototyping Journal, 2012. **18**(6): p. 482-489.

7. Murr, L.E., et al., *Metal Fabrication by Additive Manufacturing Using Laser and Electron Beam Melting Technologies.* Journal of Materials Science & Technology, 2012. **28**(1): p. 1-14.

8. Simson, T., et al., *Residual stress measurements on AISI 316L samples manufactured by selective laser melting*. Vol. 17. 2017.

9. Arısoy, Y.M., et al., *Influence of scan strategy and process parameters on microstructure and its optimization in additively manufactured nickel alloy 625 via laser powder bed fusion.* The International Journal of Advanced Manufacturing Technology, 2017. **90**(5): p. 1393-1417.

10. Liu, Y.J., et al., *Microstructure, defects and mechanical behavior of beta-type titanium porous structures manufactured by electron beam melting and selective laser melting.* Acta Materialia, 2016. **113**: p. 56-67.

11. Kruth, J.P., et al., *Selective laser melting of iron-based powder.* Journal of Materials Processing Technology, 2004. **149**(1-3): p. 616-622.

12. Wessel, J.K., *The Handbook of Advanced Materials: Enabling New Designs*. 2004: Wiley.

13. Parthasarathy, J., B. Starly, and S. Raman, *A design for the additive manufacture of functionally graded porous structures with tailored mechanical properties for biomedical applications.* Journal of Manufacturing Processes, 2011. **13**(2): p. 160-170.

14. Song, R.-b., J.-y. Xiang, and D.-p. Hou, *Characteristics of Mechanical Properties and Microstructure for 316L Austenitic Stainless Steel.* Journal of Iron and Steel Research, International, 2011. **18**(11): p. 53-59.

15. Metals, A.S., *Stainless Steel- Grade 316L - Properties, Fabrication and Applications* in *AZO Materials* 2004.

16. Bartolomeu, F., et al., *316L stainless steel mechanical and tribological behavior—A comparison between selective laser melting, hot pressing and conventional casting.* Additive Manufacturing, 2017. **16**: p. 81-89.

17. Zeng, K., *Optimization of support structures for selective laser melting* Electronic Thesis and Dissertations 2015.

18. Li, R., et al., *316L Stainless Steel with Gradient Porosity Fabricated by Selective Laser Melting.* Journal of Materials Engineering and Performance, 2009. **19**(5): p. 666-671.

19. ASTM *E92-17*, in *Standard Test Methods for Vickers Hardness and Knoop Hardness of Metallic Materials* 2017, ASTM International West Conshohocken, PA.

20. *ASTM E8/E8-13*, in *Standard Test Methods for Tension Testing of Metallic Materials* 2013, ASTM International West Conshohocken, PA.